Nondestructive superresolution imaging of defects and nonuniformities in metals, semiconductors, dielectrics, composites, and plants using evanescent microwaves

M. Tabib-Azar[a] and P. S. Pathak
Electrical Engineering and Applied Physics Department, Case Western Reserve University, Cleveland, Ohio 44106

G. Ponchak
NASA Lewis Research Center, Cleveland, Ohio 44135

S. LeClair
Air Force Research Laboratory, Materials and Manufacturing Directorate, Wright–Patterson Air Force Base, Ohio 45433

(Received 24 September 1997; accepted for publication 23 February 1999)

We have imaged and mapped material nonuniformities and defects using microwaves generated at the end of a microstripline resonator with 0.4 μm lateral spatial resolution at 1 GHz. Here we experimentally examine the effect of microstripline substrate permittivity, the feedline-to-resonator coupling strength, and probe tip geometry on the spatial resolution of the probe. Carbon composites, dielectrics, semiconductors, metals, and botanical samples were scanned for defects, residual stresses, subsurface features, areas of different film thickness, and moisture content. The resulting evanescent microwave probe (EMP) images are discussed. The main objective of this work is to demonstrate the overall capabilities of the EMP imaging technique as well as to discuss various probe parameters that can be used to design EMPs for different applications. © *1999 American Institute of Physics.* [S0034-6748(99)00406-2]

I. INTRODUCTION

Evanescent fields have been used to resolve features smaller than the classical Abbé limit. Both evanescent optical waves and microwaves have been used in high-resolution imaging to resolve features several times smaller than the wavelength of radiation.[1–10] We have shown that it is experimentally possible to obtain a lateral resolution of around 0.4 μm at 1 GHz operating frequency[8] using a tapered microstripline resonator with a fine wire tip. This lateral spatial resolution was 200 times better than our first reported resolution.[6] According to our estimations, 0.01 μm resolution imaging using high frequency evanescent microwaves probes (EMPs) operating at 10 GHz is possible.[7]

Evanescent fields are used in other frequency regimes as well.[11–15] Near-field scanning optical microscopes (NSOMs) use evanescent fields to provide resolution on the order of 10–100 Å using light of 6000 Å wavelength.[11] Atomic resolutions are achieved by using evanescent electron wave functions in scanning tunneling microscopy (STM).[14] Bethe was the first to use microwave evanescent fields to calculate the coupling coefficient of waveguides connected by a hole much smaller than the wavelength.[1] Several other experiments have demonstrated microwave near-field scanning microscopy, achieving resolutions of several thousandths of a wavelength.[5,10] These fields have been produced at the end of a coaxial resonator[5] by drilling a small hole in a waveguide[1,10] or at the end of a coaxial line.

Evanescent microwaves complement electronic and optical microscopes in the range of 0.01 μm–1 cm. The advantage of microwaves is their ability to image subsurface features in poorly conducting materials, and bulk properties due to greater penetration depth in insulators. Large scale mapping of uniformities in materials can be performed by this method. Since it is a noncontact, noninvasive, and nondestructive method, it will be very useful in the semiconductor fabrication environment.

Microwaves have some advantages over ultrasonic testing of insulators. Electromagnetic waves have relatively high transmission coefficients across solid-air boundaries in comparison to ultrasound. Also, the ultrasound absorption coefficients for dielectrics are much higher than those for microwaves.[16] Additionally, the piezoelectric effect used in ultrasonic testing diminishes at higher temperatures. Microwave testing, on the other hand, is noncontact and is ideal for high temperature testing in most materials. Thus, with microwaves we can scan hot and moving objects. Moreover, testing can be done in air, liquid, or vacuum with suitable probe characterization and essentially no sample preparation is required.

Characterization by microwaves is not limited to conducting or semiconducting media, making it a very versatile tool and useful for looking at a wide range of materials. We have experimented with samples covering the entire conductivity range (metallic to insulating) including biological specimens. Table I gives a comparison of some commonly used characterization techniques. It shows the versatility of evanescent microwaves in being useful for a wide range of

[a]Electronic mail: mxt7@po.cwru.edu

TABLE I. Comparison of some common methods for material characterization using the evanescent microwave microscope.

Method	Resolution	Conductivity limits	Comments
Optical microscopy	1–10 nm	No requirements on conductivity	For high resolution the probe needs to be a few nm from the sample; a 250 μm×250 μm scan takes 30 s
Scanning electron microscopy	100 nm[a]	Limited to materials that are conductive	Vacuum sample preparation; charging on nonconductive samples can be avoided by using a thin metal layer; expensive instruments
Scanning tunneling microscopy	Atomic level[a]	Good electron or ionic conductivity required	No free electrons involved so can be conducted in air/liquid/vacuum; field of view of only a few μm^2; 300 nm×300 nm area scan takes 10 min
Atomic force microscopy	Crystallized hard material: atomic biological: 2 nm[b]	No requirements on conductivity	Surface preparation required; both contact and noncontact methods exist
X ray	5 μm (sub-μm with synchrotron)[c]	No limitations	Poor sensitivity to the surface. Sample preparation required. Expensive and huge equipment
Ultrasonics	Order of 1 mm[d]	No requirements	Intimate coupling required due to poor transmission over boundaries; not useful at high temperatures
Eddy current	50 μm[e]	Sample should be conducting	Cannot detect planar cracks in the plane of the eddy; complicated coil designs for some applications
Evanescent microwave	~0.4 μm–1 cm[f]	Penetration depth limits bulk probing in metals	Good for large scale mapping; hot and moving samples can be imaged; no sample preparation; can be used in air/liquid/vacuum.

[a]Reference 14.
[b]Reference 15.
[c]Reference 17
[d]Reference 16.
[e]Reference 18.
[f]References 6–9.

conductivity. Large scale mapping of materials with a resolution of up to 0.01 μm is possible with evanescent microwaves by using higher frequencies of operation. Methods with higher resolution than this have the disadvantage of being incompatible for detecting large-scale inhomogeneities over large areas.

Our research in evanescent microwave imaging has concentrated on using microstriplines (shown in Fig. 1), striplines,[7] and other two-dimensional waveguide structures[9] that have the following unique advantages.

(a) The resolution of the EMP can be engineered over a wide range by using different microwave substrate thicknesses and dielectric constants, tapering angles, feedline-to-resonator coupling strengths, and various apertures in addition to frequencies. We discuss some of these design parameters in Sec. II.

(b) EMP can be integrated with silicon micromachined parts to produce miniature parallel and compact probes.

The main objectives of the work reported here are to discuss some of the probe parameters that can be used to improve the probe's resolution in a given application. We report new experimental data taken on organic and inorganic materials with conductivities ranging from metallic to insulating. These images show the versatility of the EMP and its potential application in many seemingly unrelated areas such as cancerous tissue research, bone studies, nondestructive testing of airplane parts, imaging of defects and nonuniformities in composite materials, imaging moisture and other variations in botanical samples, and imaging impurities and residual stress in semiconductors.

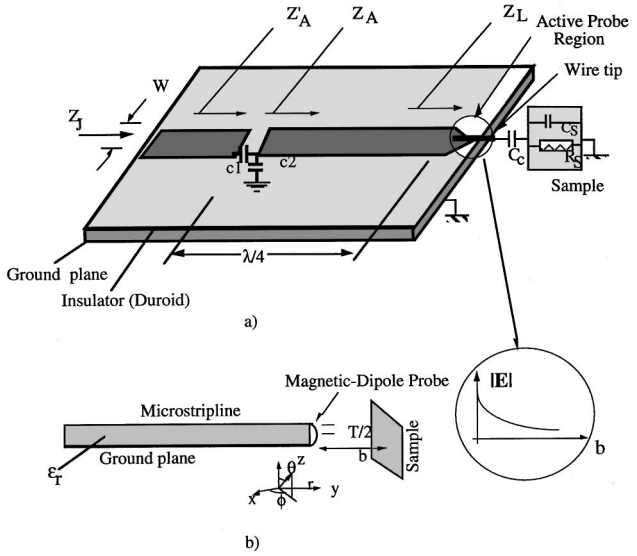

FIG. 1. (a) Microstripline resonator and probe assembly. Evanescent waves extend out of the tapered tip of the resonator. (b) The magnetic dipole probe is modeled as a microstripline with a short length of current carrying wire. The electric dipole probe is shown in (a).

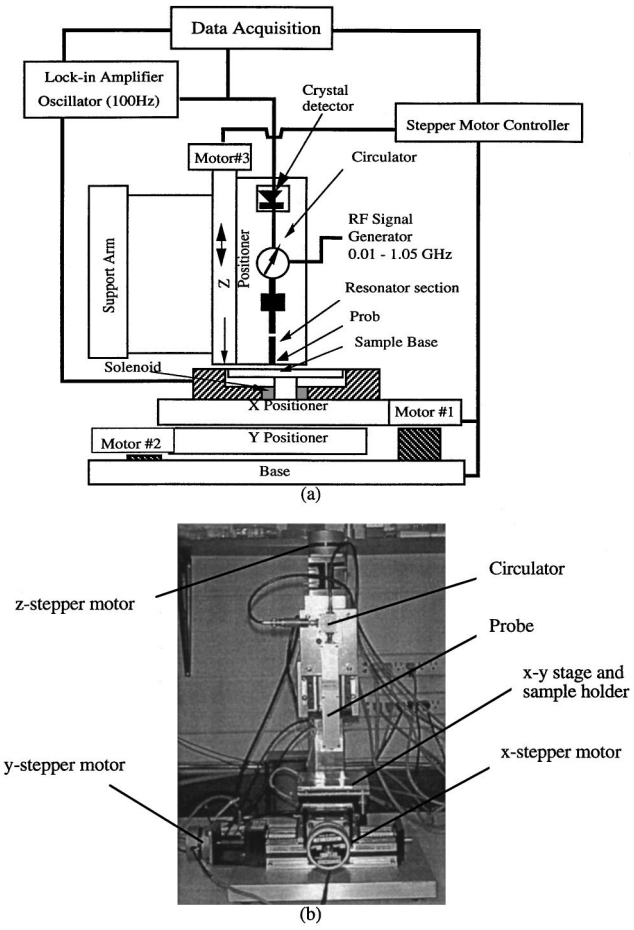

FIG. 2. (a) Schematic of the experimental setup. (b) The probe housing and the $x-y-z$ scanner arrangement.

II. EXPERIMENTAL PROCEDURE

The experimental setup used in the present work is shown in Fig. 2 and it is similar to the setup previously reported.[6] It consists of a microwave resonator coupled to a feedline, shown in Fig. 1, which is connected to a circulator. The circulator is also connected to a 0.01–1.05 GHz signal generator and to a crystal microwave detector. The detector output is a dc voltage proportional to the magnitude of the reflected wave. This is fed to an amplifier and thence to a lock-in amplifier. The probe is mounted vertically over an $x-y$ stage [Fig. 2(b)]. The $x-y$ state and the frequency generator are controlled by a personal computer. The computer also acquires data from the lock-in amplifier.

The resonator spectra were obtained using an automated network analyzer (HP 8712). The network analyzer was also used in the characterization, design, and tuning of the microwave probe.

Figure 3 shows the shift in the experimental resonance frequency with a copper plate placed near the probe tip. Both the resonance frequency and the quality factor depend on the conductivity of the sample located near the tip.[6–9] We use these dependencies to characterize materials. In metal samples defects and stresses can locally change the conductivity, and hence can be detected by the microwave probe. In the case of semiconductors the probe output can be affected by variations in carrier density, interface trap density, defects, the presence of mobile or fixed charges, grain boundaries, and variations in film thickness. In an earlier work, changes in the reflection coefficient amplitude as a function of microwave frequency and carrier concentration in Si have been reported.[6] For composites, their mechanical, chemical, and physical properties influence a change in the permittivity of the material and can be detected as a change in the reflection coefficient. In magnetic materials (ferromagnets, etc.) the variations in the permeability can be detected. These are discussed in Sec. V. We discuss the probe parameter next.

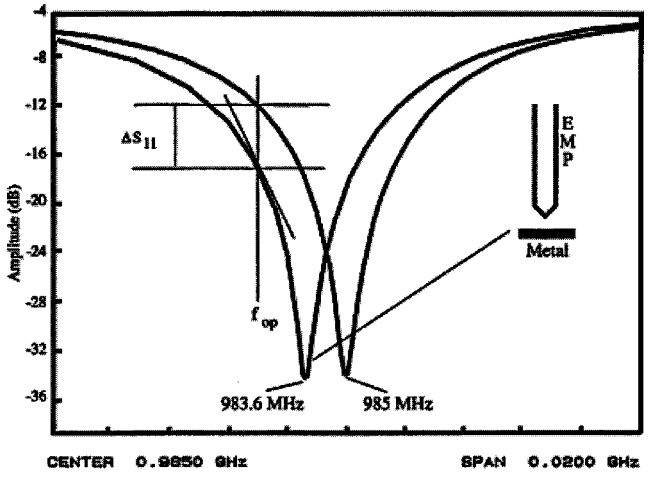

FIG. 3. The presence of a copper plate close to the probe shifts the resonant frequency by 2.4 MHz. ΔS_{11} is the change in the probe's output at f_{op}.

III. PROBE PARAMETERS

The EMP, as shown in Fig. 1, consists of a resonator fabricated on Duroid substrates. The resonator is coupled to a short feedline by an interdigitated coupling capacitor. This capacitor can be varied to tune the coupling to the resonator. The top of the resonator is tapered to localize the evanescent fields. The spatial extension of these fields, shown inside the circle in Fig. 1(a), determines the resolution of the probe.

Figure 4 shows the current density distribution at 0.93 GHz (near resonance) determined using the full-wave analysis (using SONNET) of the stripline EMP with a perfect metallic strip [Fig. 4(a)] and a resistive sample [Fig. 4(b)] located in its vicinity. In the resistive sample, the large current densities are concentrated at the region closer to the probe tip as expected. Regions in the sample with considerable current densities dominate the probe–sample interaction. From Fig. 4 it is clear that the interactions are localized in the vicinities of the probe tip regions, indicating the origin of the high spatial resolution of the EMP. The main questions that one encounters in designing planar EMPs that are based on resonators are

(1) type of waveguide and resonator configuration,
(2) substrate and waveguide parameters,
(3) probe configurations and tip geometry, and
(4) frequency of operation.

Different planar waveguide configurations include microstripline, stripline, and coplanar. We discussed the stripline EMPs in Refs. 6–8 and coplanar EMPs are presented in

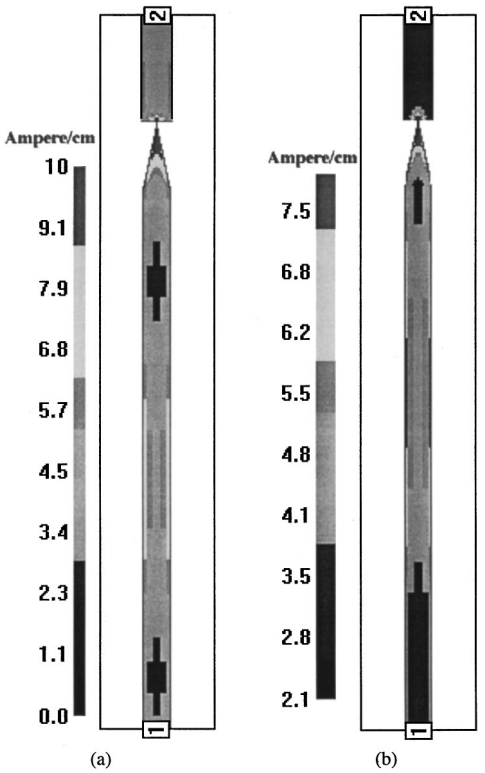

FIG. 4. (a) Current density distribution in a stripline probe with a tapered tip located near a perfect metallic sample. (b) Current density distribution in a stripline probe with a tapered tip located near a resistive metallic sample with 16.77 Ω/sq resistivity. The stripline probe in these simulations had a 2 mm dielectric ($\epsilon_r=4$) superstrate and a 1 mm dielectric ($\epsilon_r=4$) substrate. Its characteristic impedance was designed to be 50 Ω at resonance.

Ref. 9. Different resonator structures of importance in our applications include linear and ring (circular) resonators. The bulk of our work has dealt with linear microstripline resonators, an example of which is shown in Fig. 1. We will discuss ring resonators in a future publication.

Substrate parameters include thickness and permittivity. Substrate thickness and its permittivity directly affect the microstripline's capacitance per unit length (C). Linewidths affect the resonator's inductance per unit length (L). Our probes were designed to have 50 Ω characteristic impedance at resonance. To keep this impedance fixed at 50 Ω ($=L^{0.5}/C^{0.5}$), high substrates permittivities resulted in narrow linewidths.

The waveguide parameters include linewidths and feedline-to-resonator coupling strength. These are discussed in detail later.

The probe tip is usually tapered to confine the electromagnetic fields to improve the probe's resolution (Fig. 1). A fine wire can also be attached to the tapered end of the probe to reach higher spatial resolutions. When the fine wire tip is terminated in the free space, an electric dipole probe results [Fig. 1(a)]. Alternatively, if the fine wire forms a loop and is terminated at the ground plane of the resonator, a magnetic dipole probe results [Fig. 1(b)]. Electric probes have relatively high impedances and they are better suited to the characterization of insulators and semiconductors. On the other hand, magnetic probes have lower impedances and are better suited to the characterization of metals and low-resistivity materials. An aperture can also be used to confine the fields at the probe tip.

The frequency of operation determines the resonator size, field distributions at the probe tip, and the penetration depth of these fields in materials (the so called ''skin depth''). At lower frequencies, the fields have higher spatial extensions at the tip (the decay length of the field is directly proportional to the square root of wavelength) and their penetration depth is larger in conductors (the skin depth is directly proportional to the wavelength$^{0.5}$). The trade-off is smaller resolution and larger resonator and probe sizes at lower frequencies.

We have used a variety of substrate materials including Duroid, SiO_2, Si_3N_4, and high-resistivity Si. Duroid substrates offer a wide range of relative permittivities and thicknesses.

Higher permittivity substrates resulted in smaller linewidths of the microstripline for 50 Ω characteristic impedance and have higher spatial resolutions. This was experimentally verified as shown in Fig. 5.

Figure 5(a) shows the decay in the reflection coefficient with distance for the electric dipole probe for circuits on substrates with two different permittivities. The near-field decay characteristic length for the probe with substrate relative permittivity of $\epsilon_r=10.8$ is approximately 60 μm, while it is 400 μm for $\epsilon_r=2.2$. The near-field decay characteristic length for the probe is measured from the falloff in the probe response as it is moved away in the z direction (Figs. 1 and 2). In these measurements, the resonator tip was not tapered.

In the case of the magnetic dipole probe there is not much difference between different substrates, as shown in Fig. 5(b) because the probe is essentially a small loop of wire driven by the microstripline resonator. The current in the loop generates the magnetic field that interacts with the sample. Substrates with different dielectric constants do not appreciably affect the profile of this magnetic field. The slight difference between the decay constants that is observed in Fig. 5(b) is primarily due to the difference in thickness of the different substrates that results in a different size loop.

The spatial decay length (equivalent to the vertical spatial resolution) was shorter in the case of the magnetic dipole probe compared to the electric dipole probe when the substrate permittivity was low [Fig. 5(c)]. On the other hand, when the substrate permittivity was large, the electric dipole probe had a smaller decay length than the magnetic dipole probe [Fig. 5(d)].

The coupling strength changes the Q of the resonator, Fig. 6. Overcoupled resonators have poor Q, this being the reason for their lower dynamic range. For resonators with equal Q, the larger the shift in resonant frequency when a sample is brought in from infinity the larger the dynamic range. Experiments show that, for resonators made on the smaller permittivity substrate, undercoupling provides a greater shift in the resonant frequency than critical coupling. This makes undercoupled resonators on smaller permittivity substrates a better choice for imaging at larger distances. This is reasonable because for lower permittivity substrates the fields extend out to a larger area. However, for circuits on

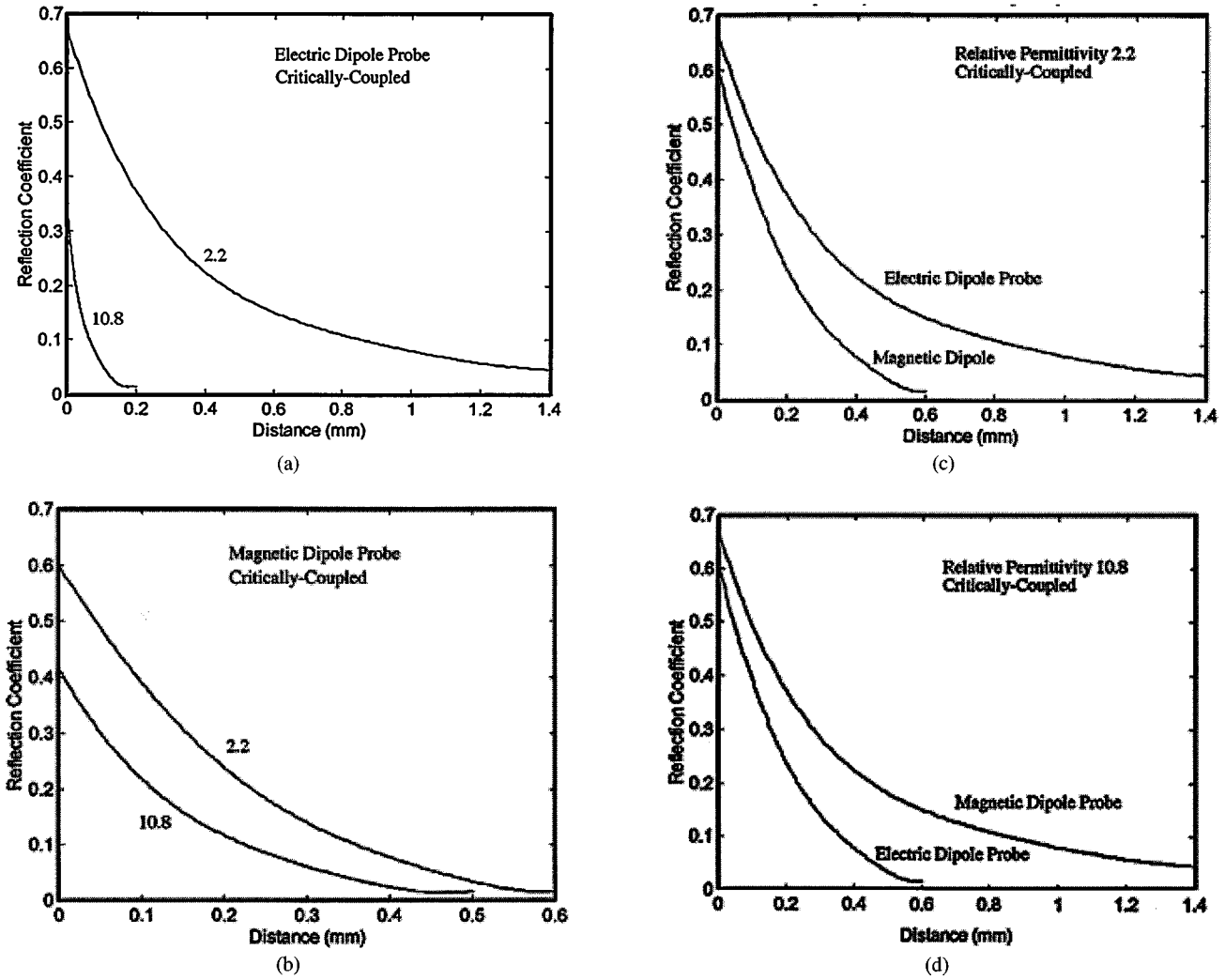

FIG. 5. Comparison of decay characteristics for a critically coupled (a) electric dipole probe and (b) a magnetic dipole probe on Duroid with two different permittivities. Comparison of the decay characteristics for the critically coupled electric and magnetic dipole probes on two different substrates with relative permittivities of (c) 2.2 and (d) 10.8.

the larger permittivity substrate the critically coupled resonator provides a larger dynamic range. So for resolving small features the critically coupled probe on a high permittivity substrate is better.

Figure 7 shows the decay characteristics for electric probes with resonators that have different coupling strengths fabricated on substrates with $\epsilon_r = 2.2$. The results were similar in substrates with higher permittivities. Both critical and

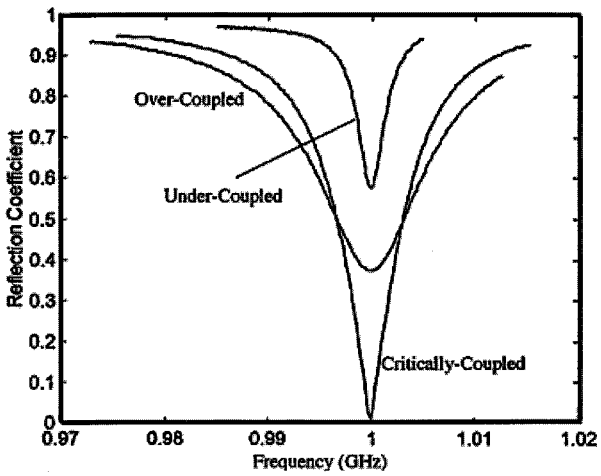

FIG. 6. Effect of coupling on the Q of the resonator. Poor Q for the over-coupled resonators reduces the dynamic range of the probe output.

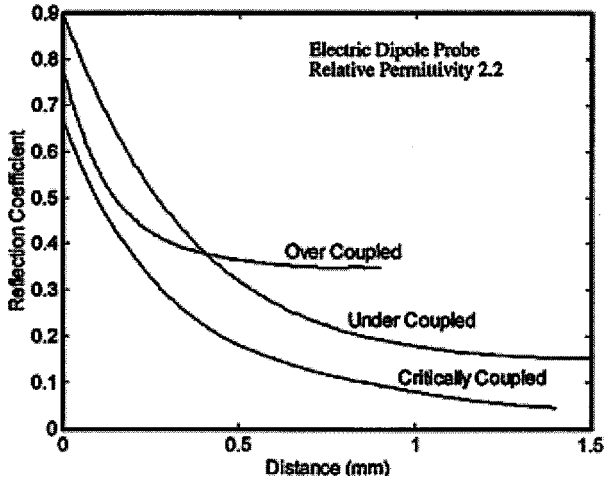

FIG. 7. Decay characteristics of the EMP for under, over-, and critically coupled electric dipole probe.

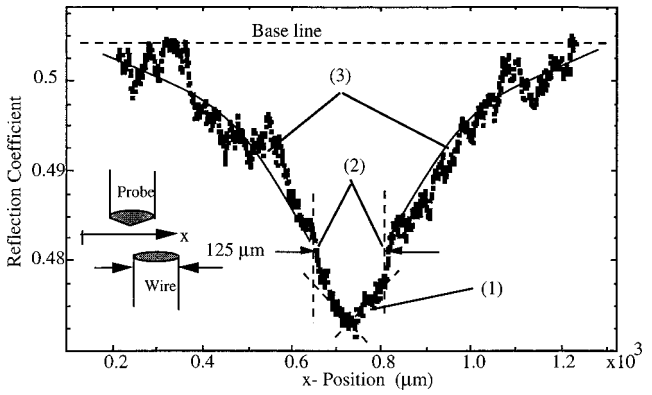

FIG. 8. Linescan over the top surface of a wire with a 125 μm diameter. In this scan a small piece of wire with a 125 μm diameter was attached to the EMP to improve its resolution.

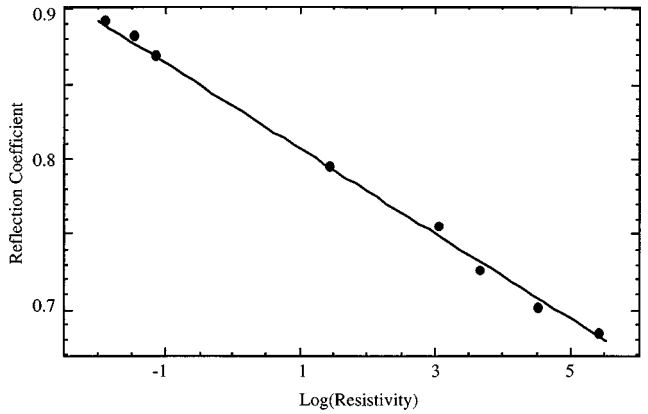

FIG. 9. Evanescent microwave probe output as a function of resistivity of the sample. The direction of change of the probe is output with resistivity depends on the relationship of the operating frequency with the center frequency of the resonator.

undercoupling provide a larger dynamic range for changes in probe-to-sample distance. The overcoupled resonator is not good in comparison. The critically coupled resonator on Duroid of $\epsilon_r = 2.2$ is good for longer ranges, with a characteristic decay length of about 500 μm.

Although probes on Duroids with 10.8 relative permittivity have higher spatial resolution, the losses are somewhat higher due to their smaller linewidths. Therefore most of the probes that were used in our work had 2.2 and 5.5 relative permittivity Duroid substrates. As discussed in Ref. 8, we achieved 0.4 μm lateral spatial resolution by tapering the probe tip (approximately 60° taper angle) and by using a fine wire (wire diam=25 μm with a tip smaller than 0.1 μm) attached to the tapered probe. The wire tip was scanned at a very small tip-to-sample distance over a polysilicon sample.[7,8] The probe resolution in the lateral directions is directly determined by the field profiles at its tip while its depth resolution is limited to the penetration depth of fields in the material that is being scanned.

Figure 8 shows a linescan of wire tip with 125 μm diameter over a wire of the same diameter. The resulting linescan has a 125 μm full width at approximately 0.68 of its minimum. The linescan shown in Fig. 8 has three different parts; (i) a linear region (1), (ii) a steep region (2), and (iii) an exponentially varying region (3). Over region (1) the signal is mainly affected by the overlap of the wire tip area and the sample area. As this overlap becomes smaller, the signal changes accordingly. The dependence of the wire overlap area on the distance between the center of the two cylindrical wires (probe wire and the sample wire) is approximately linear. The steep region (2) occurs when the overlap area becomes zero. At this point in the scan, the coupling capacitance between the wire tip and the sample wire is only due to the fringing fields. The exponentially varying region (3) is due to the near-field interaction between the probe and the sample. The decay characteristic length of this region is approximately 150 μm. In some probes, region (2) is absent. Figure 8 clearly indicates that the resolution of this probe is limited by the diameter of the wire.

IV. SAMPLE PARAMETERS

The probe output is determined by many different parameters including the frequency of operation, the probe-to-sample distance, and the electromagnetic properties of the sample. The probe-to-sample distance dependence is most problematic in situations where the sample nonuniformities, and not its topography, is to be mapped. The frequency of operation is usually set at a fixed value that corresponds to the maximum probe sensitivity and approximately linear probe response as shown in Fig. 3. The probe output dependence on the distance and the sample's electromagnetic parameters is derived and thoroughly discussed in Ref. 6. In a recent article we have also extended our previous studies and presented a circuit model and calculated the theoretical spatial and conductivity/permittivity resolution of various probe configurations.[7]

It is possible to model the response of the probe to sample resistivity using simplified circuit parameters, shown in Fig. 1(a). The sample has an impedance, which would be zero for perfect conductors and $(1+j)R_s$ for semiconductors and imperfect conductors. The characteristic impedance is $(\mu/\epsilon)^{0.5}$ for lossless dielectrics and it can be approximated as

$$\sqrt{\frac{\mu}{\epsilon}}\left\{\left[1-\frac{3}{8}\left(\frac{\epsilon''}{\epsilon'}\right)^2\right]+j\,\frac{\epsilon''}{2\epsilon'}\right\}$$

for lossy dielectrics. Here $\epsilon' - j\epsilon''$ is the complex permittivity, and ϵ'/ϵ'' is assumed to be much less than 1. It is also well known that the variations in the local conductivity of the sample can be due to variations in carrier concentrations, thickness of the films, defects, interface traps, stresses, impurities, and moisture content. The permittivity can vary due to local variations in atomic polarizability.

The change in probe output with resistivity is shown in Fig. 9. The four-point probe resistivity of different samples was measured and the evanescent microwave probe output at $f_{op} = 1.014$ GHz (center frequency of 1.011 GHz), corresponding to these points, is plotted versus the resistivity. The probe output falls with an increase in resistivity. The magnitude and sign of the slope of probe output versus sample resistivity will depend on the operating frequency and its location with respect to the center frequency on the resonance curve.

V. MATERIAL CHARACTERIZATION

We have imaged samples with a wide range of conductivities. The results of our scans over dielectrics, semiconductors, metals, and biological specimens are discussed below. The experimental data presented here have been obtained from two-dimensional scans over the samples. After being acquired the data were deconvolved with the field profile at the tip of the probe. Then this was pseudocolored by assigning the continuous voltage ranges a red, green, and blue (rgb) color.

The field profile was estimated by using the linescan of Fig. 8 as follows. The ''spreading'' in the wire's profile in our scan was due to the interaction of the evanescent fields with the wire. The algorithm for the discrete deconvolution was developed using a simple observation that the signal at any point on the sample is affected by the residual interaction of the evanescent fields with the adjacent neighboring points. Knowing the evanescent field profile, the total contribution to the signal at any point from its nearest neighbors is estimated and subtracted from the raw signal at that point. This process was repeated for every point and a new image was constructed. In most cases this deconvolution process resulted in a sharper image compared to the raw image. A detailed description of this method is forthcoming.

By deconvolving the experimental wire scan with the wire's physical profile we get an ''effective'' field profile which includes the effect of the probe tip dimension and any other factors which influence spreading in the probe resonance. This profile is then used to extract features from our two-dimensional scans. By curve fitting we estimated the field profiles to drop off as $e^{-r/r_0}/r$, where r_0 is the lateral characteristic decay length, and it varies from probe to probe. By curve fitting, using a least mean square error estimate of good fit, one can estimate r_0 for a probe from its linescan response to a wire. For typical probes operating at 1 GHz it varied from 125 to 1 μm.

A. Dielectrics

Figure 10(a) shows a microwave resistivity image over a 2×3 mm^2 region of a carbon composite. Scans over intact and delaminated sections of this composite depict a marked change in the probe response pattern. In the delaminated sample the image pattern is much more fragmented, indicating large variations in the microwave properties of the composite. Darker regions in this image correspond to lower effective density, and hence lower permittivity regions, while lighter region in the image correspond to denser and higher permittivity regions in the composite.

Figure 10(b) shows defects in a BN sample. The darker regions in this image correspond to lower permittivity regions than the rest of the BN sample by as much as 50% ($\Delta\epsilon/\epsilon=0.5$).

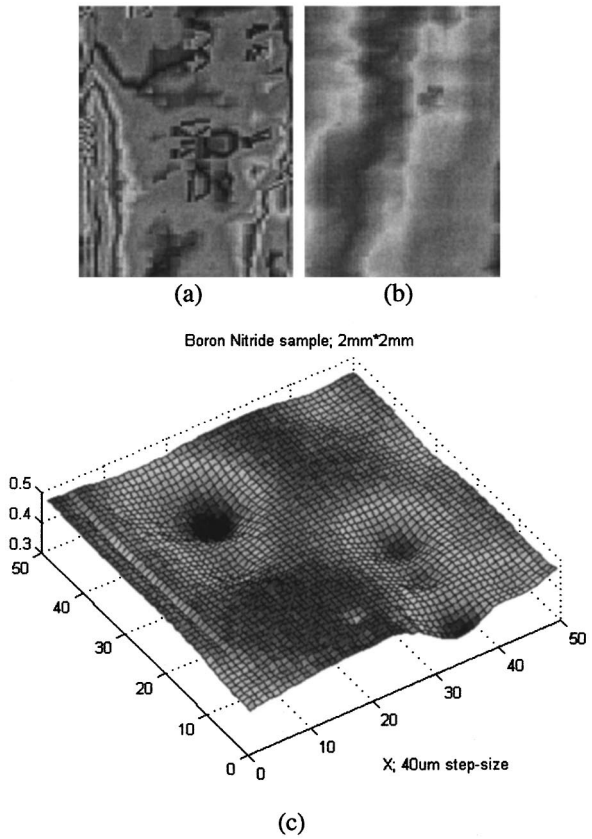

FIG. 10. (a) Delaminated and intact composites imaged side by side show that it is possible to detect delaminations using the EMP. The region on the left corresponds to the delaminated composite with darker regions having lower density corresponding to lower permittivity. The scanning was done at 1 GHz using a critically coupled electric dipole probe. 30×30 points were scanned over a 2×3 cm^2 area. (b) EMP image of defects in the BN sample. The defective regions (shown as dark depressions) had lower permittivities than rest of the sample by as much as 50% ($\Delta\epsilon/\epsilon=0.5$).

B. Semiconductors

Figure 11(a) is a two-dimensional pseudocolored scan of a 4 in. 1.5 μm 3C-SiC on a Si wafer. The results were exciting because the pseudocolored plot of the scan shows variations on the wafer which matched the resistivity map obtained by four-point probe measurements.[19]

Since the microwave probe response is quite fast (<0.1 μs), the response of the semiconductor to an external stimulus, such as an optical pulse or a depleting high-power electromagnetic pulse, can be monitored. Figure 11(b) shows an oscilloscope trace of the EMP's output response of a silicon sample. A switched optical pulse generated by a GaAs laser diode was used in this experiment. These transient measurements can be performed at different temperatures and, since the microwave probe measurement is noncontact, only the semiconductor sample needs to be cooled or heated. Thus, activation energies and various parameters of deep levels, such as their capture/emission cross sections and densities, can be determined. The carrier recombination lifetime, calculated from the transient response of the EMP in Fig. 11(b), was approximately around 2 ms in the B-doped silicon sample with a 100 Å gate oxide.

C. Metals

Figure 12 shows an optical and a microwave image of a 2 mm diam hole in a copper plate. A linescan over the same hole [Fig. 12(c)] can detect burrs on the edge of the hole. Earlier it has been reported[10] that for small features (less than

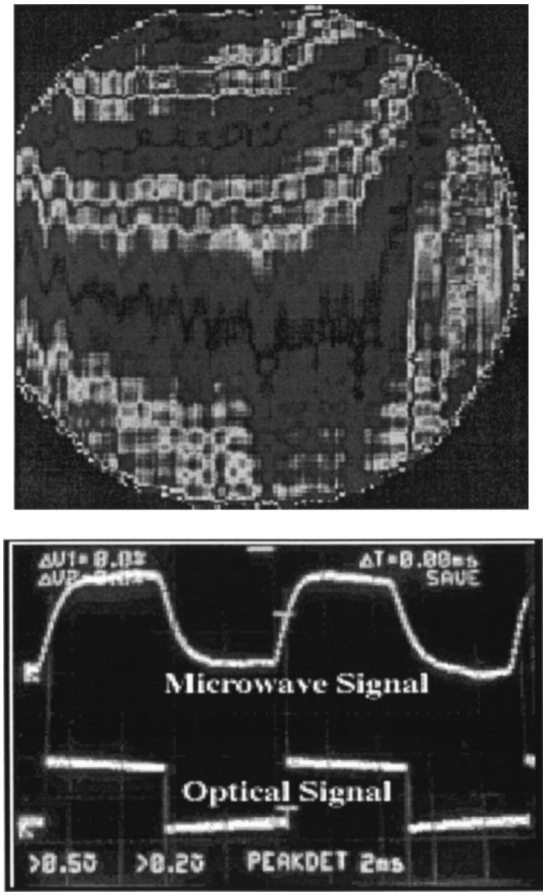

FIG. 11. (a) Evanescent microwave image of a 4 in. 3C-SiC/Si wafer. Variations in film thickness/resistivity due to the gas flow are detected by the evanescent microwave probe. The scan consists of 130×130 points over the wafer. The resistivity in this wafer varied between 1 (white) and 10 Ω cm (black). (b) Carrier lifetime measurement using the EMP. The carrier recombination lifetime (≈2 ms in this case) can be calculated from the transient behavior of the EMP output when the optical pulse is turned off.

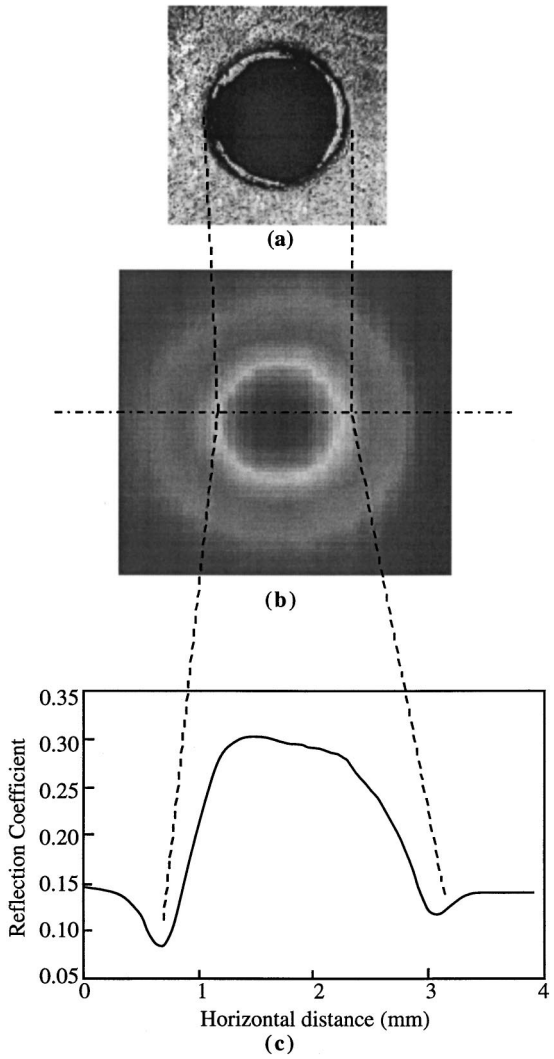

FIG. 12. (a) Optical micrograph of a 2 mm diam hole in a 6 mm thick copper plate. (b) An EMP image of the same hole. (c) A linescan over the 2 mm diam hole can detect burrs at the edges of a hole in the copper plate. The burr width was 89 μm.

0.5 mm) the probe gives double peaks due to asymmetry in the fields. But the peaks seen in this linescan at the edges of the hole are not found in scans over other similar holes, implying that they are due to the burrs on the edge of the hole. Scans over grooves of known depth in the same copper plate were also taken to characterize the probe's output with respect to the depth of the strips. In Table II we compare the depth and width measurements of these copper grooves, made using the evanescent microwave probe to the actual depths and widths.

In Fig. 13 we have the microwave probe output at different points along a metal component with a known stressed region. Residual stress in metals causes an increase in random carrier scattering, resulting in lower local conductivities in the stressed regions. In this case (Fig. 13) the local conductivity in the stressed region changed by as much as $\Delta\sigma/\sigma = 10^{-4}$.

D. Magnetic materials

Figure 14 shows a pseudocolor EMP image of a magnetic disk. Due to the permeability variations across the magnetic domains, the EMP is capable of detecting these regions. The dark areas in Fig. 14 correspond to higher permeability than the light areas. In this measurement, an electric dipole probe was used. It is possible to perform these measurements

TABLE II. Comparison of actual values of the depths and widths of grooves in a copper plate to those measured using the evanescent microwave probe.

Groove	Experimental depth (mm)	Actual depth (mm)	Experimental width (mm)	Actual width (mm)
First	0.133±0.012	0.145	5.175±0.300	4.875
Second	0.134±0.016	0.150	5.413±0.525	4.888
Third	0.320±0.011	0.331	5.125±0.225	4.9

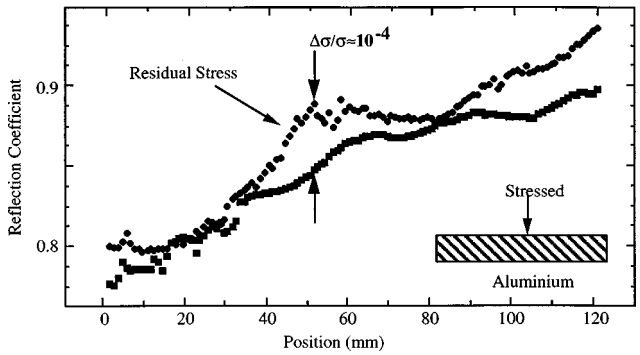

FIG. 13. The microwave probe detects stress in a component. The metal piece was stressed to introduce residual stress. Stress detection is possible because of variations in the subsurface conductivity due to stresses.

in the presence of an externally applied magnetic field. The implication of such high spatial resolution magnetization measurements in data storage/retrieval is quite clear.

E. Biological specimens

Figures 15(a) and 15(b) show optical images of a plant leaf and a corresponding pseudocolored EMP image of a small region in this leaf. The moisture content as well as some basic features of the leaf can be detected using our probe. This technique, being noncontact, noninvasive, nondestructive, and capable of operating in any medium, is ideal for studying biological specimens in buffer solutions and in air. We are currently in the process of performing imaging of soft (skin) and hard (bone) biological tissues.

Figure 15(c) and 15(d) show optical images of balsa wood and its corresponding EMP image. Regions of higher moisture content in this balsa wood can be seen as white regions in the EMP image. With more refined EMP measurements it should be possible to detect the mineral contents as well as density variation in woods and other similar hierarchical materials.

VI. DISCUSSION

We discussed some of the issues involved in the design of evanescent microwave probes and explored the application of these probes in studying various materials. Microwave substrates with higher permittivities usually resulted in more confined fields in the electric dipole probes. Thus, the spatial resolution of these probes was higher than the probes with smaller permittivities. The magnetic dipole probes' resolutions did not show the same dependence on substrate

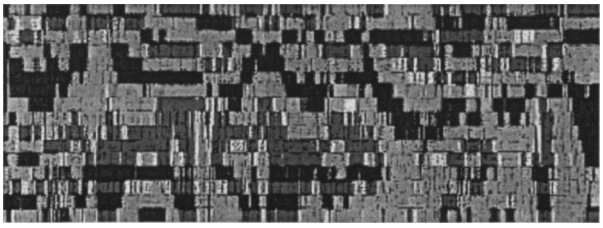

FIG. 14. Map of magnetic domains of a hard drive disk obtained using EMP imaging. This image clearly shows the ability of the EMP to detect variations in the permeability of the magnetic disk. Dark areas have higher permeability than light areas.

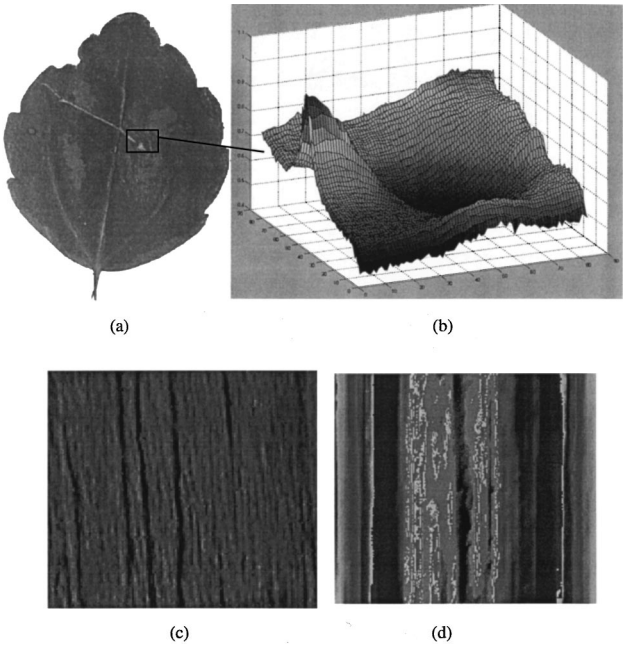

FIG. 15. (a) Optical image of a plant leaf. (b) EMP scan of a small area of the plant lead. (c) Optical image of balsa wood (2×1 cm^2). (d) EMP scan of the same balsa wood clearly showing regions containing moisture (white areas).

permittivity. We explained this lack of appreciable dependence by noting that the magnetic field profiles are predominantly determined by the radius of the wire loops that form these probes and that the loop size can be set more or less independent of the substrate permittivities. The EMP was capable of imaging conductivity variation and recombination lifetimes in semiconductors. It also yielded information regarding nonuniformities in metals (regions having residual stress), insulators (BN), composites (delaminated versus intact parts), a plant leaf, and balsa wood. The EMP is capable of imaging materials in noncontact mode and nondestructively through air or other suitable media and, hence, it has many potential applications in biological and botanical material studies.

ACKNOWLEDGMENTS

The authors thank Steve Pelkowski and Vince Gatto for their work on Figs. 5–7, A. Boozer for her contribution to microwave imaging of metallic samples, and Se-Ho You for his contribution to Fig. 15(b). This work was partially supported by Wright–Patterson Air Force Base and by the NASA Lewis Research Center.

[1] H. A. Bethe, Phys. Rev. **66**, 163 (1944).
[2] R. F. Soohoo, J. Appl. Phys. **33**, 1276 (1962).
[3] E. A. Ash and G. Nicholls, Nature (London) **237**, 510 (1972).
[4] R. J. Gutmann, J. M. Borrego, P. Chakrabarti, and M.-S. Wang, IEEE Microwave Theory Tech. 281 (1987).
[5] M. Fee, Steven Chu, and T. W. Hansch, Opt. Commun. **69**, 219 (1989).
[6] M. Tabib-Azar, N. S. Shoemaker, and S. Harris, Meas. Sci. Technol. **4**, 583 (1993).
[7] M. Tabib-Azar, G. Ponchak, and S. LeClair, Rev. Sci. Instrum. (submitted).

[8] D.-P. Su, A. Pohar, and M. Tabib-Azar, Rev. Sci. Instrum. **70**, 1725 (1999).
[9] G. E. Ponchak, D. Akinwande, and M. Tabib-Azar, IEEE Microwave Theory Tech. 5 (submitted).
[10] T. Wei, X. D. Xiang, W. G. Wallace-Freedman, and P. G. Schultz, Appl. Phys. Lett. **68**, 3506 (1996).
[11] U. Durig, D. W. Pohl, and F. Rohrer, J. Appl. Phys. **59**, 3318 (1986).
[12] C. J. R. Sheppard, Proc. SPIE **368**, 88 (1972).
[13] R. J. Stephenson, Rev. Sci. Instrum. **67**, 3891 (1996).
[14] U. Memmert, U. Hodel, and U. Hartmann, Rev. Sci. Instrum. **67**, 2269 (1996).
[15] J. Mou, J. Yang, and Z. Shao, Rev. Sci. Instrum. **64**, 483 (1993).
[16] J. Ylitalo, Ultrasonics **34**, 331 (1996).
[17] T. Noma and A. Iida, Rev. Sci. Instrum. **65**, 837 (1994).
[18] K. Wegendt, R. P. Heubener, R. Gross, Th. Trauble, W. Geweke, W. Patzwaldt, W. Prusseit, and H. Kinder, Cryogenics **35**, 155 (1995).
[19] C. Jacob, S. Nishino, P. Pirouz, C. A. Zorman, A. J. Fleischman, and M. Mehragany, *International Conference on Silicon Carbide and Related Materials*, 1995 (ICSCRM-95), September 18–21, Kyoto, Japan.